IJE TRANSACTIONS A: Basics Vol. 35, No. 04, (April 2022) 635-643

International Journal of Engineering

Journal Homepage: www.ije.ir

Evaluation of Corrosion Resistance of Bi-layered Plasma-sprayed Coating on Titanium Implants

N. Ebrahimi, A. Sedaghat Ahangari Hosseinzadeh*, M. Vaezi, M. Mozafari

Materials and Energy Research Center, Karaj, Iran

P A P E R I N F O

Paper history:
Received 16 November 2021
Received in revised form 15 December 2021
Accepted 23 December 2021

Keywords:
Coating
Plasma Spraying
Corrosion
Porosity

A B S T R A C T

There are several attempts to improve surface characteristics of biomaterials with thick film coatings. In this research, a class of protective coating layers of bi-layered Hydroxyapatite (HA)/Al_2O_3-SiO_2 (with 10, 20, 30 %wt SiO_2) were deposited on titanium (Ti) surfaces by plasma spray technique. The surface features of the applied coating layers were evaluated in detail to confirm the effectiveness of the technique for further biomedical applications. The results demonstrated that uniform and bi-layered plasma sprayed coatings can be successfully prepared through the optimization of engineering parameters. Also, it was found that the roughness of the bi-layered coatings increases with increasing the number of coating layers. The corrosion behavior of the coated and uncoated samples was comparatively investigated using electrochemical tests. The measured current densities (i_{corr}) for HA, (HA)/Al_2O_3-SiO_2 (with 10, 20, 30 %wt SiO_2) were 0.27μA/cm^2, 0.28 μA/cm^2, 0.23 μA/cm^2, 0.79 μA/cm^2, respectively. According to the results, corrosion resistance of samples with 20% SiO_2 is significantly improved compared to the single-layer HA and bare Ti. The outcomes of FESEM results revealed that porosity and cavities related to evaporation of adhesive PVA and it is confirmed by increasing the percentage of silica to more than 20%, porosity has increased. In conclusion, the proposed coating system showed promising abilities for future biomedical applications. It could be optimized and improved by changing the structural characteristics of the substrate, chemical composition and porosity of the coating layers.

***doi**: 10.5829/ije.2022.35.04a.03*

NOMENCLATURE

FESEM	Field emission scanning electron microscopy	FTIR	Fourier-transform infrared spectroscopy
R_p	Polarization resistance	EDS	Energy-dispersion X-ray Spectroscopy
I_{corr}	Current density	SBF	Simulated body fluids
βa	Anodic tafel slope	PE	Protection efficiency
βc	Cathodic tafel slope	PVA	poly-vinyl alcohol
P	Total porosity of the coating	XRD	X-ray diffraction
R_{pm}	Polarization resistance of the un-coated sample	TCP	Tricalcium phosphate
R_p	Polarization resistance of the coated sample	α-TCP	α-$Ca_3(PO_4)_2$
ΔE_{corr}	Different potential of the coated sample and the bare substrate	β-TCP	β-$Ca_3(PO_4)_2$
λ	Wavelength of X-ray beam	HA	Hydroxyapatite
β	Maximum intensity of the full width at half maximum	Ti	Titanium
Θ	Diffraction angle	AT	Al_2O_3–TiO_2
K	Constant selected at 0.9	EPD	Electrophoretic deposition
l	Average crystallite size		

1. INTRODUCTION

Compared with other metallic biomaterials titanium (Ti) and its alloys have become the most pleasant metallic materials used in orthopaedic implants because of the high corrosion resistance and favorable biocompatibility properties [1, 2]. Alloys used as implants should not show any unfavorable physiological responses in body

* Corresponding Author Institutional Email: a.sedaghat@merc.ac.ir
(A. Sedaghat Ahangari Hosseinzadeh)

Please cite this article as: N. Ebrahimi, A. Sedaghat Ahangari Hosseinzadeh, M. Vaezi, M. Mozafari, Evaluation of Corrosion Resistance of Bi-layered Plasma-sprayed Coating on Titanium Implants, ***International Journal of Engineering, Transactions A: Basics*** Vol. 35, No. 04, (2022) 635-643

environment and should be *chemically* stable.[3] The passive layer established on the surface of titanium alloys indicates the long-term stability after exposure in body which has a great influence on biocompatibility [4]. However, osseointegration and bone growth on implants are also influenced by the level of bioactivity of titanium alloys that could be varied by the type of the alloys and processing conditions. Modification of surfaces often improved the interactions between tissue and implant substrate [5, 6]. Calcium phosphate-based biomaterials have been shown a bone like chemical composition and porous structure. Although these biomaterials such as HA ($Ca_{10}(PO_4)_6(OH)_2$) showed superior bioactive properties for orthopedic and clinical applications, they are restricted to nonload-bearing applications, because of their brittleness and low mechanical strength [7, 8]. Most of these implants failed after 15 years of implantations in the body due to weak resistance against wear and corrosion. One of the greatest effective surface modifications is applying a coating on the surface to enhance the corrosion resistance of metallic implants [9]. Previous researches showed that implants modified with nano ceramics such Al_2O_3, SiO_2 and TiO_2 are generally improved in terms of corrosion behavior and biocompatibility [10-12]. A recent study by Bahraminasab et al. [13]. showed that the highest corrosion resistance of Al_2O_3- 75vol.%Ti composite caused to apply for making the components of implants such as knee and hip prostheses. In addition, Farhadian et al. [14] showed that increasing SiO_2 content improved corrosion performance of ZrO_2-SiO_2 coatings. Alumina (Al_2O_3) is a ceramic material that are used in artificial joints and hip prosthesis. This is related to superior wear resistance and excellent mechanical properties [15]. It should be noted that it is impossible to create an excellent bone grafting when Al_2O_3 is used in the body because of bioinertness and low osseointegration ability of alumina [16]. In this context, various Al_2O_3- based composites were expanded to overcome these bugs, such as HA-Al_2O_3 and Al_2O_3 –ZrO_2 composites [17, 18]. In previous researches, this result has found that by adding the SiO_2 to the substrate can improve the protective properties because of high corrosion resistance of SiO_2 [19] There is not any study about the creation of alumina-silica nanocomposite as a bond coat. So, it was considered as the main point of the present research.

Various techniques were used for application of coatings on metallic substrates, for example electrophoretic deposition (EPD), sol-gel, sputtering and plasma spraying [20-23]. Among the techniques, plasma sprayed coatings exhibit high corrosion resistance. Some parameters, such as adhesive strength between substrate and coating, elements of precursors, porosity and composition of the coatings could potentially affect corrosion behavior [24]. Compared to different coating methods, plasma spray was a simple technique and contains a wide deposition rate, widespread particle size range and exhibits high -quality coatings [25, 26].

Some studies have previously shown that during plasma spraying HA phase could be converted to α-TCP (α-$Ca_3(PO_4)_2$), β-TCP (β-$Ca_3(PO_4)_2$) or other calcium oxide phases [27]. It has been reported that rapid solidification can reduce the crystallinity degree of HA coatings [27, 28]. Also, most investigations were done to determine in vitro and in vivo properties of plasma-sprayed HA coating [29-36]. Vu et al. [29] presented that the superior bone information of ZnSiAg-HA coatings when they were implanted in 18 male Sprague-Dawley rats.

In this study, a bi-layer plasma sprayed coating consisting of HA as the top layer and Al_2O_3-SiO_2 nanocomposite with 10, 20 and 30 %wt SiO_2 as the intermediate layer on the medical grade pure titanium was established (Figure 1(a)). Adding the SiO_2 to the substrate can improve the protective properties because of high corrosion resistance of SiO_2. Afterward, microstructure, porosity and corrosion behavior of the coatings were compared with the single-layer HA coatings (Figure 1(b)) and the bare titanium substrate. The influence of the adding an intermediate layer on the electrochemical corrosion behavior of the pure titanium was evaluated by potentiodynamic polarization accompanied by Field emission scanning electron microscopy (FESEM).

2. MATERIALS AND METHODS

2. 1. Materials Commercial pure Ti (grade #2, 1×1 cm^2) was used as substrate. The chemical composition of N: 0.07, C:0.7, Fe: 0.02, O: 0.67 and others Ti, which is according to the reported data for ASTM grade #2 [24]. Prior to the plasma spraying, the substrate was degreased and grit blasted with 24 µm alumina mesh to achieve a

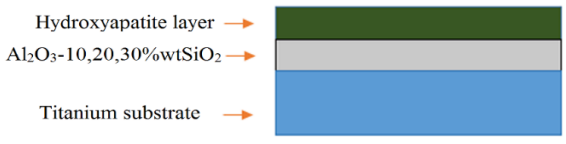

(a)

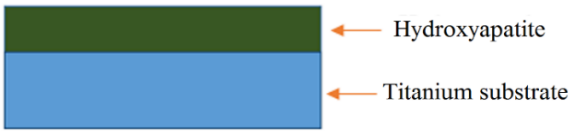

(b)

Figure 1. Schematic diagram of plasma-sprayed coatings a) bi-layered coating b) single-layered coating

rough surface (3.01-3.56 µm). Three types of powder were used in this study; α-Al_2O_3 (99%, Merck, 40-50nm), amorphous SiO_2 (99%, Merck, 15-25nm), and synthesized hydroxyapatite nanopowder (20-40nm).

Hydroxyapatite nanoparticles were synthesized by a sonochemical technique. Starting materials used for the synthesis included high-purity calcium nitrate ($Ca(NO_3)_2$-$4H_2O$) (99%, Merck), ammonium hydrogen phosphate ($(NH_4)_2HPO_4$) (99%, Merck), absolute ethanol and ammonium hydroxide. A high-intensity ultrasonic probe (Misonix S4000, Tihorn, 20 kHz, 500W/cm^2, USA) was used for the ultrasound irradiation reactor. Initially, 50 ml/mol of diammonium hydrogen phosphate was dissolved in distilled water and added drop wise to a solution of 84 mol/ml hydrated calcium nitrate in absolute ethanol at a temperature of 30 ºC. The initial power of the sonicator was set at 40 W. The reaction was carried out for 1.5 h and pH of the solution was adjusted to 10 by using an adequate amount of NH_4OH solution. After formation of slurry, the sediment was centrifuged for 10 minutes and then washed three times. The precipitate was aged at 80°C for 5 h. Finally, the obtained powder was calcined at 700 ºC with a rate of 10 K.min^{-1}.

2. 1. Plasma Spraying Process Al_2O_3 and 10, 20 and 30%wt SiO_2 powders were mixed with mechanically alloyed mixture for 3 h by using zirconia balls. In order to obtain desired flowability of nano powders and to optimize the deposition efficiency, primary nano powders were granulated with a 5%-wt poly-vinyl alcohol (PVA) solution as a binder. The powders were sieved by 140, 170, 200, 270 and 325 sieves. Size distribution of granular powders was 44-88 µm. In this work, plasma spraying was performed in air by a Plasma Metco 3MB gun (Sulzer- Metco; Switzerland). The coatings are shown schematically in Figure 1. The spraying parameters of both layers were listed in Table 1. The specimens of titanium substrates were preheated at 250 ºC to increase the adhesion strength of coatings. The amount surface roughness of uncoated pure titanium and plasma sprayed coatings was measured by TR 100 Roughness of Surface tester. Ra (the average roughness of a surface) and Rz (the difference between the highest "peak" and the deepest "valley" in the surface) are different factors of roughness. These parameters were measured at four places on surface of specimens. The average amount of these parameters was presented.

2. 3. Characterizations of Feed Stokes X-ray diffraction (XRD) was used to analyze the phases obtained from the spraying experiments. This test was performed by a PW3710-based X-ray diffraction device manufactured by Philips Netherlands under a voltage of 40 kV and 30 mA (Cu Kα, 1.5405 *Å*, scan rate: 0.02 mv/s). The crystallite size of the samples was obtained from the X-ray diffraction pattern by the Debye–Scherrer equation [32]:

TABLE 1. Plasma spray parameters (Distance: 10 cm, Ar plasma gas flow rate: 85 SCFH, H_2 plasma gas flow rate: 15 SCFH)

Sample	Composition (%)	Current (A)	Plasma voltage (V)
H	100% HA	450	55
H-A-10S	HA / Al_2O_3-10%SiO_2	450 / 500	55 / 58
H-A-20S	HA / Al_2O_3-20%SiO_2	450 / 500	55 / 58
H-A-30S	HA / Al_2O_3-30%SiO_2	450 / 500	55 / 58

$$l = \frac{K\,\lambda}{\beta\,cos\Theta} \quad (1)$$

where λ is the wavelength of X-ray beam, β is the maximum intensity of the full width at half maximum, Θ is the diffraction angle, K is constant selected at 0.9 and l is the average crystallite size.

Phase analysis was performed by Fourier-transform infrared spectroscopy (FTIR) studies of the synthesized HA nano particles. The powders and cross-section morphologies were assessed by field emission scanning electron microscope (FESEM, TESCAN MIRA3) and Energy-dispersion X-ray Spectroscopy (EDS; 15 kV). In order to investigate cross-sectional morphology, the coated samples were cut and embedded in epoxy. Then, the mounted samples were polished by SiC abrasive paper #600-#2000. A thin layer of gold was sputtered on the polished surface of samples to ensure adequate electrical conductivity during FESEM observation.

2. 4. Electrochemical Tests Polarization potentiodynamics test was performed by an Auto Lab device in simulated body fluids (SBF). Preparation of SBF solution was performed based on the protocol of Bansal et al. [26]. The electrochemical test of coating specimens was accomplished with three electrodes, the coated samples as working electrode, the saturated calomel electrode as reference electrode, and a platinum rod as counter electrode. The samples were kept in the solution for 90 min until the open circuit potential (OCP) was stabilized. All tests were measured at a potential of 0.25 -2 V with a scanning rate of 1 mV/s.

Polarization resistance was calculated from Stern Geary equation as indicated below [27]:

$$R_p = \frac{(\beta_a \times \beta_c)}{2.3 \times I_{corr} \times (\beta_a + \beta_c)} \quad (2)$$

In which R_p is polarization resistance, I_{corr} is current density, βa and βc are anodic and cathodic tafel slopes, respectively. The porosity of the plasma sprayed coatings was identified by electrochemical behavior of the coatings. The porosity was estimated by using the following relation [28]:

$$\%P = \frac{R_{pm}}{R_p} \times 10^{-\left|\frac{\Delta E_{corr}}{\beta_a}\right|} \quad (3)$$

where P is the total porosity of the coatings, R_{pm} the polarization resistance of the un-coated sample and R_p the polarization resistance of the coated sample. ΔE_{corr} is the different potential of the coated sample and the bare substrate.

The protection efficiency (PE) of the single layered and bi-layered coatings were obtained from the following relation [29]:

$$PE = \frac{(R_p - R_{pm})}{Rp} \times 100 \quad (4)$$

where R_p and R_{pm} are related to polarization resistance of the coated and uncoated samples respectively.

3. RESULTS and DISCUSSION

3. 1. FTIR and XRD Analysis In this study a modified-sonochemical technique used to synthesize HA nanoparticles with increasing calcination temperature and decreasing reaction time compared to that of conventional sonochemical technique. FTIR analysis of the synthesized HA nanoparticles has been performed in the range of 400 cm^{-1} to 4000 cm^{-1} as shown in Figure 2. Vibrations of 3563 cm^{-1}, 3423 cm^{-1} bands and peaks around 632 cm^{-1} demonstrated the presence of hydroxyl groups. The presence of CO_3^{-2} groups was observed at 1458 cm^{-1} , 1418 cm^{-1} and 870 cm^{-1} .Bands located at 565 cm^{-1} and 603 cm^{-1} indicated the stretching vibrations of the phosphates group, and the tensile vibrations of the phosphate were measured at 1095 cm^{-1}, 1046 cm^{-1} and 962 cm^{-1}. The result of FTIR Spectra was in agreement with prior literature [37-39].

Figure 3 (a) shows XRD pattern of synthesized HA nanoparticles. The diffraction peaks are typical for the HA structure in accordance with the JCPDS standard card 00-009-0432. The XRD patterns indicate that the ultrasound waves are more impressive to achieve pure HA nanoparticles when calcination temperature was kept at 700 ºC. The XRD pattern (Figure 3 (a)) shows only HA crystallite phase. The crystallite size was assessed 15-25 nm.

Figure 4 indicates XRD pattern of Al_2O_3-10%SiO_2 nanocomposite after 3 h ball milling. All the sharp peaks correspond to α-Al_2O_3 and the broadened peak at an angle of 15 to 25 degrees indicates the amorphous silica phase. According to previous research, the x-ray diffraction pattern of SiO_2 powder is made of one broadened peak that is identified Si– O– Si groups of amorphous SiO_2 [14]. By using the Scherrer equation as presented in Equation 1, the alumina crystallite size was calculated to be 45-65 nm.

The XRD pattern of HA/Al_2O_3-10%SiO_2 also is shown in Figure 3(b). By comparison the pattern of the HA before and after coating, it is observed that the tricalcium phosphate (TCP) and calcium oxide phases are formed during coating process. The dissolution degree of these phases as follows [32]:

Ca> TCP > HA

TCP has been found to dissolve more in physiological solutions, as well as displaying a greater rate of dissolution or degradation than HA, when implanted in body environment [32]. Other researchers have also offered that the tricalcium phosphate and calcium oxide

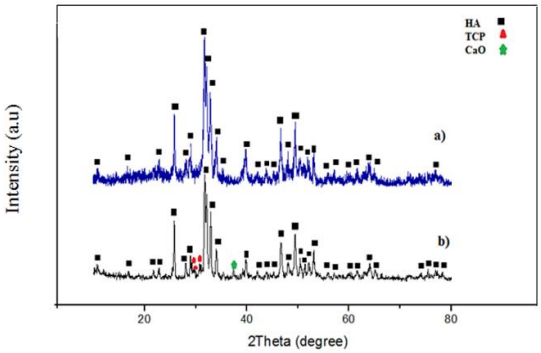

Figure 3. XRD pattern of (a) synthesized HA nanoparticles b) H-A-20S plasma-sprayed coating sample

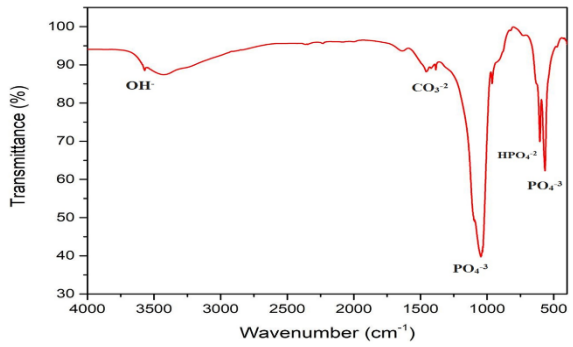

Figure 2. FTIR analysis of hydroxyapatite synthesized nanopowder

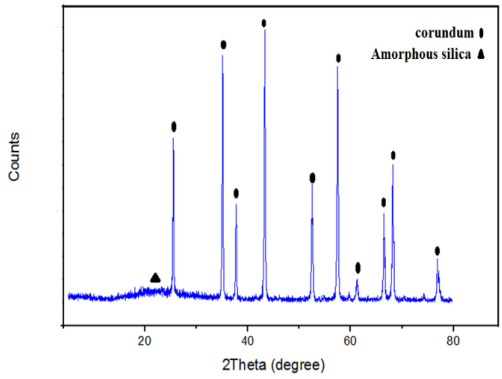

Figure 4. X-ray diffraction pattern of Al_2O_3-10%SiO_2 nanocomposite

phases can be composed [33, 34]. The remarkable thing is the high mass absorption coefficient of the HA compared to corundum and silica phases and it causes the phases formed in the middle layer are not recognizable in this pattern. The mass absorption coefficient of the HA, corundum and silica was calculated and obtained 502.33, 101.96, and 60.08 cm^2/g, respectively. On the other hand, X-rays won't go through a thick coating. The X-ray diffraction pattern was taken from a coated sample without the HA layer for assessing the presence of corundum phase and other phases formed in the intermediate layer. The presence of the corundum (α-Al_2O_3) and mullite can be observed in the XRD pattern of Al_2O_3-10%SiO_2 coating without the top coat which is in accordance to cards 01-071-1123 and 00-015-0776 respectively, is revealed in Figure 5.

3. 2. Microstructure and Cross Sectional Analysis

Figure 6 shows morphology of the granulated HA and Al_2O_3-10%SiO_2 nanocomposite powders. The granulated powders have spherical and semi-spherical morphology. The EDS spectra of the Al_2O_3-10%SiO_2 nanocomposite also depicted 42.62% Al, 4.69% Si and 43.44% oxygen (Figure 6(c)). The nano powders do not have the ability to spray by plasma spraying due to the lack of adequate fluidity. Some portion of the nanoparticles should be melted because mechanical behavior of the coating is strongly related to melting degree of sprayed particles [35].

Scanning electron microscopy images of the plasma-sprayed samples are shown in Figure 7. Also, the thickness of the coatings is presented in Table 2. The cross-sectional images of the coatings indicated good adhesive bonding with substrate and no cracks are seen at the interface of coating and substrate. During the plasma spraying, the particles are exposed to a high temperature. Then, the powders are well sintered and they have fused together. HA layer and Al_2O_3- SiO_2 nanocomposite with 10, 20 and 30 percent of SiO_2

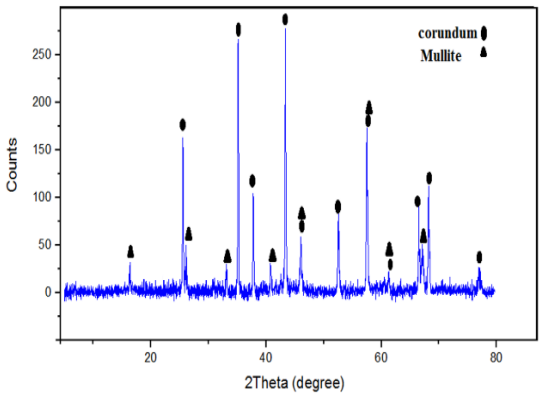

Figure 5. XRD pattern of plasma-sprayed Al_2O_3-20%SiO_2 coating without top coat

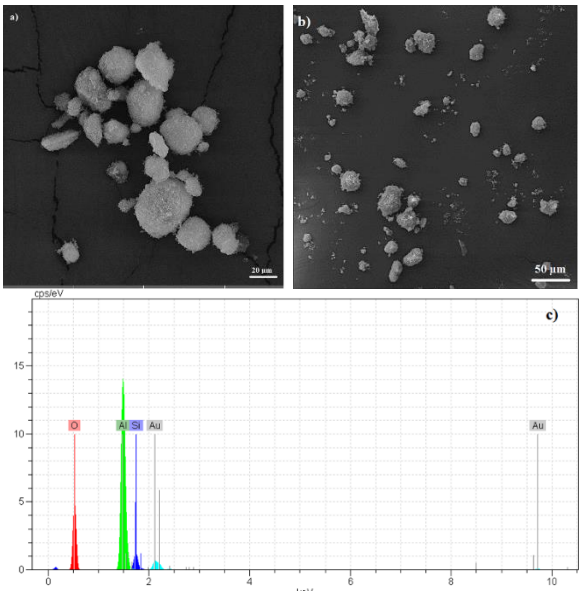

Figure 6. Scanning microscopic image of granulated powder of (a) HA b) Al_2O_3-10%SiO_2 nanocomposite Cc) EDS of nanocomposite

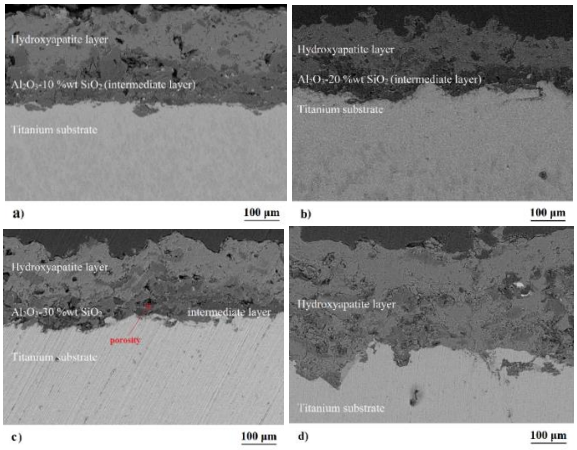

Figure 7. Cross-sectional images of plasma-sprayed coatings (a) H-A-10S (b) H-A-20S (c) H-A-30S (d) H

exhibited the lamellar structure. The porosity and cavities can be observed, which can be due to the evaporation of adhesive PVA. By image analysis of the high-resolution images, it can be concluded that H-A-30S coating displays more pores. The HA and H-A-20S coatings exhibit dense and low amount of the porosity. Also H-A-10S sample showed the distribution number of pores. It is clear that by increasing the percentage of silica to more than 20%, porosity has increased. Velocity of powder feeding, distance of the gun from the metal substrate and particle size are influencing melting of the particles during the plasma spraying [36]. The presence of the porosity, unmelted, semi-melted zones and cracks in the thermal sprayed coating also revealed in previous studies

[37, 38]. For example, Song et al. [39] showed increase in critical plasma spray parameter results in decrease in volume fractions of pores and partially melted regions, and consequently raises the overall hardness of the coatings. The overall hardness increase generally leads to decrease in wear rate.

It is observed that the nanostructured powders are porous and this inherent porosity will be maintained in the microstructure of the plasma-sprayed coatings. Lima et al. [40] discovered that the un-molten and nanostructured powders influence the elastic modulus, hardness, and thermal conductivity properties. Yılmaz [41]evaluated plasma-sprayed coatings on pure titanium substrate. It was observed that it is possible to coat Al_2O_3 and Al_2O_3–13 wt.% TiO_2 on pure titanium substrate by using atmospheric plasma-spray process for determined conditions [42]. EDS Mapping of H-A-10S specimen is given in Figure 8. It shows the distribution of Al, Si, O, P, Ca and Ti in the sample. As expected, Ca and P are present in the upper layer. The mechanism of plasma-spray process can cause the presence of the titanium in the coating. But it is not noticeable.

3. 3. Polarization Studies The electrochemical behavior of the titanium substrate coated by HA and Al_2O_3-10, 20, 30%wt SiO_2 was evaluated in simulated body fluids. The observed polarization plots of different plasma sprayed coatings are indicated in Figure 9. The corrosion parameters, such as current, potential corrosion, porosity and polarization resistance, which were calculated by the Stern Geary equation are presented in Table 3. It is clear that the corrosion currents of the coated samples decreased compared to the uncoated titanium. According to the polarization curves, it is considered that the current density of H-A-20S sample is lower than other samples. The corrosion potential and current density of H-A-20S are -468 mV and 0.23 μA/cm^2, respectively, are shown in Figure 9. Also, amount of β_a and β_c were obtained 372.79 mV/dec and 182.73 mV/dec, respectively. Therefore, the polarization resistance was calculated 230498.6 Ω/cm^2.

The amount of porosity is very important for the corrosion resistance of coatings. The measured porosity of coated samples is listed in Table 3. The highest porosity is related to H-A-30S. Also, H-A-20S coating contain low porosity compared to H-A-30S and H-A-10S. The current density of H-A-30S is more than other coatings.

TABLE 2. The measured thickness of the top coat and intermediate coat

Samples	Thickness top coat (μm)	Thickness intermediate coat (μm)
H	150-180	-
H-A-10S	100-130	90-100
H-A-20S	80-90	50-60
H-A-30S	80-100	50-60

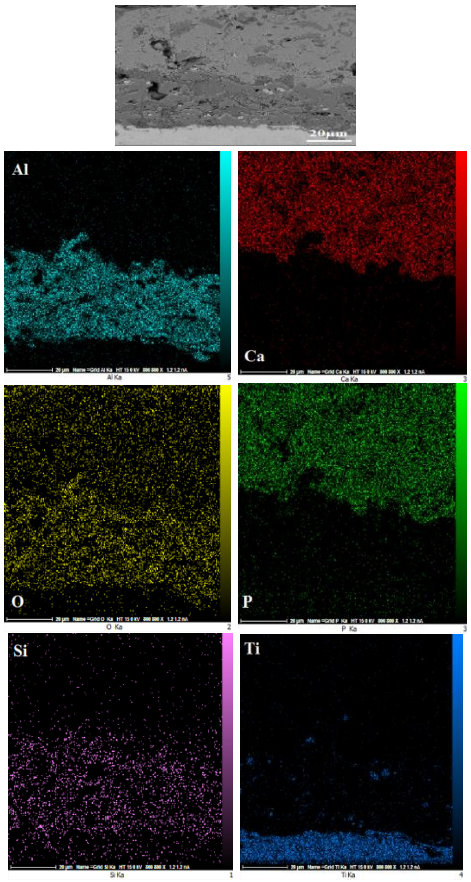

Figure 8. Cross-sectional images of plasma-sprayed coatings a) H-A-10S b) H-A-20S c) H-A-30S d) H

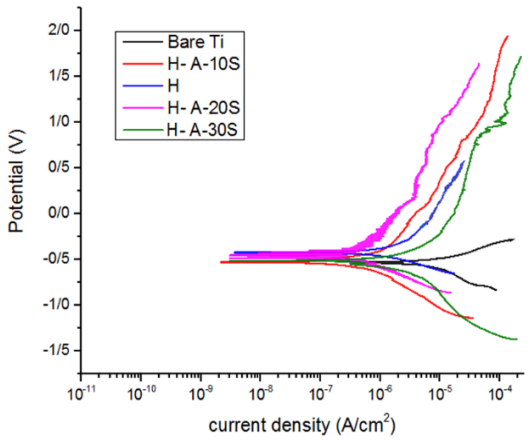

Figure 9. Potentiodynamic polarization curves of plasma-sprayed coating in SBF solution

TABLE 3. Corrosion parameters measured from polarization curves in SBF solution

Samples	Bare Ti	H	H-A-10S	H-A-20S	H-A-30S
β_a (mV/dec)	93.85	77.40	254.20	372.79	194.82
β_C (mV/dec)	145.71	67.23	209.40	182.73	221.02
i_{corr} ($\mu A/cm^2$)	3.25	0.27	0.28	0.23	0.79
E_{corr} (mV)	-529	-420	-510	-468	-496
R_p (Ω/cm^2)	7627.1	56402.5	177884.6	230498.6	56770.1
% Porosity	-	1.0	3.0	0.8	5.8
% PE	-	86.4	95.7	96.6	76.5

In fact, the high porosity increased corrosion current and reduced polarization resistance. The porosity, un-molten and semi-molten particles, pores and microstructural properties affected on the current density and corrosion resistance. Increased porosity goes along with increased corrosion rates. This is an effect of accessible surface area, which increases with increasing porosity [43]. The presence of pores and channels allow deeper penetration of the fluid, which, again, increases the corrosion rate. It is observed that addition of the intermediate coat with chemical composition of Al_2O_3-20%wt SiO_2 increased corrosion resistance compared to the pure titanium and the single layer HA coating. Actually by increasing in the silica content of more than 20%, corrosion resistance has been reduced. The high presence of porosities in the microstructure of H-A-30S because of wide particle size distribution that cause to segregate during injection into the plasma jet. Smaller particles may not penetrate fully into the plasma jet, decreasing the deposition quality and increasing the porosity cause to low corrosion resistance [44, 45]. Usually, the intrinsic defects of plasma-sprayed coatings, for example pores (porosity), partially melted particles or un-molten and cracks have destructive on the mechanical, physical and chemical properties of the coatings [46-53]. The protection efficiency of H, H-A-10S, H-A-20S and H-A-30S coatings were obtained 86.47, 95.71, 96.69 and 76.56% respectively.

4. CONCLUSIONS

The present study revealed the use of an intermediate coat with the composition of Al_2O_3-20% wt SiO_2 applied with the plasma spray technique on the surface of titanium implant. This led to considerable improvements in the corrosion resistance due to the presence of the intermediate coat (corundum and mullite) with low porosity. The corundum, mullite, TCP and CaO phases without surplus phases were observed in the XRD patterns of the coatings. Electrochemical studies showed desirable corrosion resistance of the double-layer H-A-20S coating. Increased porosity (H-A-30S coating) goes along with increased corrosion rates. The presence of pores and channels allow deeper penetration of the fluid, which, again, increases the corrosion rate. In conclusion, the plasma-sprayed double-layer coatings can be used as protective coating systems for dental and orthopedic implants.

5. ACKNOWLEDGMENTS

The present study was supported by Materials and Energy Research Center (MERC) through grant No. 344596.

6. REFERENCES

1. Bai, Y., Deng, Y., Zheng, Y., Li, Y., Zhang, R., Lv, Y., Zhao, Q., Wei, S.J.M.S. and C, E., "Characterization, corrosion behavior, cellular response and in vivo bone tissue compatibility of titanium–niobium alloy with low young's modulus", ***Materials Science and Engineering: C***, Vol. 59, (2016), 565-576, doi: 10.1016/j.msec.2015.10.062
2. Zhang, L.C. and Chen, L.Y.J.A.e.m., "A review on biomedical titanium alloys: Recent progress and prospect", ***Advanced Engineering Materials***, Vol. 21, No. 4, (2019), 1801215, doi: 10.1002/adem.201801215
3. Qosim, N., Supriadi, S., Puspitasari, P. and Kreshanti, P.J.I.J.o.E., "Mechanical surface treatments of Ti-6Al-4v miniplate implant manufactured by electrical discharge machining", ***International Journal of Engineering, Transactions A: Basics***, Vol. 31, No. 7, (2018), 1103-1108. doi: 10.5829/ije.2018.31.07a.14
4. Yu, S. and Scully, J.J.C., "Corrosion and passivity of ti-13% nb-13% zr in comparison to other biomedical implant alloys", ***Corrosion***, Vol. 53, No. 12, (1997), doi: 10.5006/1.3290281
5. Kokubo, T.J.B., "Hm kim and m. Kawashita", ***Biomaterials***, Vol. 24, (2003), 2161, doi: 10.1016/S0142-9612(03)00044-9
6. Ermis, M., Antmen, E. and Hasirci, V.J.B.m., "Micro and nanofabrication methods to control cell-substrate interactions and cell behavior: A review from the tissue engineering perspective", ***Bioactive Materials***, Vol. 3, No. 3, (2018), 355-369, doi: 10.1016/j.bioactmat.2018.05.005
7. Shirdar, M.R., Izman, S., Kheimehsari, H.M., Ahmad, N. and Ma'aram, A.J.S.I., "Evaluation of mechanical and electrochemical properties of fha-coated co–cr implant", ***Surface Innovations***, Vol. 5, No. 2, (2017), 90-96, doi: 10.1680/jsuin.16.00028
8. Singh, J., Chatha, S.S. and Singh, H., "Synthesis and characterization of plasma sprayed functional gradient bioceramic coating for medical implant applications", ***Ceramics International***, Vol. 47, No. 7, (2021), 9143-9155, doi: 10.1016/j.ceramint.2020.12.039
9. Bordbar-Khiabani, A., Yarmand, B. and Mozafari, M.J.S.I., "Functional peo layers on magnesium alloys: Innovative polymer-free drug-eluting stents", ***Surface Innovations***, Vol. 6, No. 4–5, (2018), 237-243, doi: 10.1680/jsuin.18.00011

10. Çomaklı, O., Yazıcı, M., Yetim, T., Yetim, A. and Çelik, A.J.C.I., "Effect of ti amount on wear and corrosion properties of ti-doped Al_2O_3 nanocomposite ceramic coated cp titanium implant material", ***Ceramics International***, Vol. 44, No. 7, (2018), 7421-7428, doi: 10.1016/j.ceramint.2018.01.046
11. Xu, J., Joguet, D., Cizek, J., Khor, K.A., Liao, H., Coddet, C., Chen, W.N.J.S. and Technology, C., "Synthesis and characterization on atomphospheric plasma sprayed amorphous silica doped hydrxoyapatite coatings", ***Surface and Coatings Technology***, Vol. 206, No. 22, (2012), 4659-4665, doi: 10.1016/j.surfcoat.2012.05.042
12. Ebrahimi, N., Zadeh, A.S.A.H., Vaezi, M., Mozafari, M.J.S. and Technology, C., "A new double-layer hydroxyapatite/alumina-silica coated titanium implants using plasma spray technique", ***Surface and Coatings Technology***, Vol. 352, (2018), 474-482, doi: 10.1016/j.surfcoat.2018.08.022
13. Bahraminasab, M., Bozorg, M., Ghaffari, S., Kavakebian, F.J.M.S. and C, E., "Corrosion of Al_2O_3-ti composites under inflammatory condition in simulated physiological solution", ***Materials Science and Engineering: C***, Vol. 102, (2019), 200-211, doi: 10.1016/j.msec.2019.04.047
14. Farhadian, M., Raeissi, K., Golozar, M., Labbaf, S., Hajilou, T. and Barnoush, A.J.A.S.S., "3d-focused ion beam tomography and quantitative porosity evaluation of ZrO_2-SiO_2 composite coating; amorphous SiO_2 as a porosity tailoring agent", ***Applied Surface Science***, Vol. 511, (2020), 145567, doi: 10.1016/j.apsusc.2020.145567
15. Bahraminasab, M., Sahari, B.B., Edwards, K.L., Farahmand, F. and Arumugam, M., "Aseptic loosening of femoral components – materials engineering and design considerations", ***Materials & Design***, Vol. 44, (2013), 155-163, doi: 10.1016/j.matdes.2012.07.066
16. Xie, H., Zhang, L., Xu, E., Yuan, H., Zhao, F. and Gao, J.J.C.I., "Sialon– Al_2O_3 ceramics as potential biomaterials", ***Ceramics International***, Vol. 45, No. 14, (2019), 16809-16813, doi: 10.1016/j.ceramint.2019.05.22
17. Askari, N., Yousefpour, M. and Rajabi, M.J.I.J.o.A.C.T., "Determination of optimum al content in ha-al2o3 nanocomposites coatings prepared by electrophoretic deposition on titanium substrate", ***International Journal of Applied Ceramic Technology,***, Vol. 15, No. 4, (2018), 970-979, doi: 10.1111/ijac.12826
18. Jiao, C., Gu, J., Cao, Y., Xie, D., Liang, H., Chen, R., Shi, T., Shen, L., Wang, C. and Tian, Z.J.J.o.t.E.C.S., "Preparation of Al_2O_3-ZrO_2 scaffolds with controllable multi-level pores via digital light processing", ***Journal of the European Ceramic Society***, Vol. 40, No. 15, (2020), 6087-6094, doi: 10.1016/j.jeurceramsoc.2020.06.024
19. Mazur, A., Szczurek, A., Chęcmanowski, J.G., Szczygieł, B.J.S. and Technology, C., "Corrosion resistance and bioactivity of SiO_2-Y_2O_3 coatings deposited on 316l steel", ***Surface and Coatings Technology***, Vol. 350, (2018), 502-510, doi: 10.1016/j.surfcoat.2018.07.042
20. Farrokhi-Rad, M.J.J.o.A. and Compounds, "Effect of morphology on the electrophoretic deposition of hydroxyapatite nanoparticles", ***Journal of Alloys and Compounds***, Vol. 741, (2018), 211-222, doi: 10.1016/j.jallcom.2018.01.101
21. Batebi, K., Khazaei, B.A., Afshar, A.J.S. and Technology, C., "Characterization of sol-gel derived silver/fluor-hydroxyapatite composite coatings on titanium substrate", ***Surface and Coatings Technology***, Vol. 352, (2018), 522-528, doi: 10.1016/j.surfcoat.2018.08.021
22. Akbari, G., Nikravesh, M. and Poladi, A.J.I.J.o.E., "Mechanical properties and microstructural evolution of ta/tanx double layer thin films deposited by magnetron sputtering", ***International Journal of Engineering, Transactions B: Applications***, Vol. 30, No. 2, (2017), 288-293, doi: 10.5829/idosi.ije.2017.30.02b.16
23. Ren, J., Zhao, D., Qi, F., Liu, W. and Chen, Y.J.J.o.t.m.b.o.b.m., "Heat and hydrothermal treatments on the microstructure evolution and mechanical properties of plasma sprayed hydroxyapatite coatings reinforced with graphene nanoplatelets", ***Journal of the Mechanical Behavior of Biomedical Materials***, Vol. 101, (2020), 103418, doi: 10.1016/j.jmbbm.2019.103418
24. Celik, E., Ozdemir, I., Avci, E., Tsunekawa, Y.J.S. and Technology, C., "Corrosion behaviour of plasma sprayed coatings", ***Surface and Coatings Technology***, Vol. 193, No. 1-3, (2005), 297-302, doi: 10.1016/j.surfcoat.2004.08.143
25. Gkomoza, P., Vardavoulias, M., Pantelis, D., Sarafoglou, C.J.S. and Technology, C., "Comparative study of structure and properties of thermal spray coatings using conventional and nanostructured hydroxyapatite powder, for applications in medical implants", ***Surface and Coatings Technology***, Vol. 357, (2019), 748-758, doi: 10.1016/j.surfcoat.2018.10.044
26. Bansal, P., Singh, G., Sidhu, H.S.J.S. and Technology, C., "Investigation of surface properties and corrosion behavior of plasma sprayed ha/zno coatings prepared on az31 mg alloy", ***Surface and Coatings Technology***, Vol. 401, (2020), 126241, doi: 10.1016/j.surfcoat.2020.126241
27. Bogya, E.S., Károly, Z. and Barabás, R.J.C.I., "Atmospheric plasma sprayed silica–hydroxyapatite coatings on magnesium alloy substrates", ***Ceramics International***, Vol. 41, No. 4, (2015), 6005-6012, doi: 10.1016/j.ceramint.2015.01.041
28. Noorakma, A.C., Zuhailawati, H., Aishvarya, V. and Dhindaw, B.K., "Hydroxyapatite-coated magnesium-based biodegradable alloy: Cold spray deposition and simulated body fluid studies", ***Journal of Materials Engineering and Performance***, Vol. 22, No. 10, (2013), 2997-3004, doi: 10.1007/s11665-013-0589-9
29. Vu, A.A., Robertson, S.F., Ke, D., Bandyopadhyay, A. and Bose, S.J.A.b., "Mechanical and biological properties of zno, SiO_2, and ag2o doped plasma sprayed hydroxyapatite coating for orthopaedic and dental applications", ***Acta Biomaterialia***, Vol. 92, (2019), 325-335, doi: 10.1016/j.actbio.2019.05.020
30. Girija, E., Kumar, G.S., Thamizhavel, A., Yokogawa, Y. and Kalkura, S.N.J.P.t., "Role of material processing on the thermal stability and sinterability of nanocrystalline hydroxyapatite", ***Powder Technology***, Vol. 225, (2012), 190-195, doi: 10.1016/j.powtec.2012.04.007
31. Elias, C., Lima, J., Valiev, R. and Meyers, M.J.J., "Biomedical applications of titanium and its alloys", ***JOM***, Vol. 60, No. 3, (2008), 46-49, doi: 10.1007/s11837-008-0031-1
32. Puspitasari, P. and Budi, L.J.I.J.o.E., "Physical and magnetic properties comparison of cobalt ferrite nanopowder using sol-gel and sonochemical methods", ***International Journal of Engineering, Transactions B: Applications***, Vol. 33, No. 5, (2020), 877-884, doi: 10.5829/ije.2020.33.05b.20
33. Kokubo, T. and Takadama, H.J.H.u.i.S.i.p.i.v.b.b., Biomaterial, "Leading opinion", ***Biomaterials***, Vol. 27, (2006), 2907-2915, doi: 10.1016/j.biomaterials.2006.01.017
34. Palanivelu, R., Kalainathan, S. and Kumar, A.R.J.C.I., "Characterization studies on plasma sprayed (at/ha) bi-layered nano ceramics coating on biomedical commercially pure titanium dental implant", ***Ceramics International***, Vol. 40, No. 6, (2014), 7745-7751, doi: 10.1016/j.ceramint.2013.12.116
35. Jam, A., Derakhshandeh, S.M.R., Rajaei, H. and Pakseresht, A.H.J.C.I., "Evaluation of microstructure and electrochemical behavior of dual-layer nicraly/mullite plasma sprayed coating on high silicon cast iron alloy", ***Ceramics International***, Vol. 43, No. 16, (2017), 14146-14155, doi: 10.1016/j.ceramint.2017.07.155
36. Kumar, A.M., Rajendran, N.J.S. and Technology, C., "Influence of zirconia nanoparticles on the surface and electrochemical

behaviour of polypyrrole nanocomposite coated 316l ss in simulated body fluid", ***Surface and Coatings Technology***, Vol. 213, (2012), 155-166, doi: 10.1016/j.surfcoat.2012.10.039

37. Ch, A., Sagadevan, S. and Dakshnamoorthy, A.J.I.j.o.p.s., "Synthesis and characterization of nano-hydroxyapatite (n-hap) using the wet chemical technique", ***International Journal of Physical Sciences***, Vol. 8, No. 32, (2013), 1639-1645, doi: 10.5897/IJPS2013.3990
38. Poinern, G., Brundavanam, R., Le, X.T., Djordjevic, S., Prokic, M. and Fawcett, D.J.I.j.o.n., "Thermal and ultrasonic influence in the formation of nanometer scale hydroxyapatite bio-ceramic", ***International Journal of Nanomedicine***, Vol. 6, (2011), 2083, doi: 10.2147/IJN.S24790
39. Song, E.P., Ahn, J., Lee, S., Kim, N.J.J.S. and Technology, C., "Effects of critical plasma spray parameter and spray distance on wear resistance of Al_2O_3–8 wt.% TiO_2 coatings plasma-sprayed with nanopowders", ***Surface and Coatings Technology***, Vol. 202, No. 15, (2008), 3625-3632, doi: 10.1016/j.surfcoat.2008.01.002
40. Lima, R.S., Kucuk, A. and Berndt, C.C., "Bimodal distribution of mechanical properties on plasma sprayed nanostructured partially stabilized zirconia", ***Materials Science and Engineering: A***, Vol. 327, No. 2, (2002), 224-232, doi: 10.1016/S0921-5093(01)01530-1
41. Yılmaz, Ş.J.C.I., "An evaluation of plasma-sprayed coatings based on Al_2O_3 and Al_2O_3–13 wt.% TiO_2 with bond coat on pure titanium substrate", ***Ceramics International***, Vol. 35, No. 5, (2009), 2017-2022, doi: 10.1016/j.ceramint.2008.11.017
42. Zamani, S., Salahi, E. and Mobasherpour, I.J.C.C.T., "Removal of nickel from aqueous solution by nano hydroxyapatite originated from persian gulf corals", ***Canadian Chemical Transactions***, Vol. 1, No. 3, (2013), 173-190, doi: 10.13179/canchemtrans.2013.01.03.0033
43. Ben-Nissan, B.J.A.i.C.P.B., "Advances in calcium phosphate biomaterials preface", Vol. 2, (2014), Ix-Xi, doi: 10.1007/978-3-642-53980-0
44. Singh, G., Singh, S. and Prakash, S., "Surface characterization of plasma sprayed pure and reinforced hydroxyapatite coating on Ti6Al4v alloy", ***Surface and Coatings Technology***, Vol. 205, No. 20, (2011), 4814-4820, doi: 10.1016/j.surfcoat.2011.04.064
45. Morks, M. and Kobayashi, A.J.A.S.S., "Effect of gun current on the microstructure and crystallinity of plasma sprayed hydroxyapatite coatings", ***Applied Surface Science***, Vol. 253, No. 17, (2007), 7136-7142, doi: 10.1016/j.apsusc.2007.02.183
46. Di Girolamo, G., Marra, F., Blasi, C., Serra, E., Valente, T. "Microstructure, mechanical properties and thermal shock resistance of plasma sprayed nanostructured zirconia coatings", ***Ceramics International***, Vol. 37, No. 7, (2011), 2711-2717, doi: 10.1016/j.ceramint.2011.04.024
47. Levingstone, T.J., Ardhaoui, M., Benyounis, K., Looney, L., Stokes, J.T.J.S. and Technology, C., "Plasma sprayed hydroxyapatite coatings: Understanding process relationships using design of experiment analysis", ***Surface and Coatings Technology***, Vol. 283, (2015), 29-36, doi: 10.1016/j.surfcoat.2015.10.044
48. Sun, L., Berndt, C.C., Grey, C.P.J.M.S. and A, E., "Phase, structural and microstructural investigations of plasma sprayed hydroxyapatite coatings", ***Materials Science and Engineering: A***, Vol. 360, No. 1-2, (2003), 70-84, doi: 10.1016/S0921-5093(03)00439-8
49. Abualigaledari, S., "Development of an anti-corrosion thermally sprayed coating system for oil and gas transmission pipeline", (2018).
50. Salimijazi, H., Hosseini, M., Mostaghimi, J., Pershin, L., Coyle, T.W., Samadi, H. and Shafyei, A., "Plasma sprayed coating using mullite and mixed alumina/silica powders", ***Journal of Thermal Spray Technology***, Vol. 21, No. 5, (2012), 825-830, doi: 10.1007/s11666-012-9766-x
51. Pakseresht, A., Rahimipour, M., Vaezi, M., Salehi, M.J.M.C. and Physics, "Thermal plasma spheroidization and spray deposition of barium titanate powder and characterization of the plasma sprayable powder", ***Materials Chemistry and Physics***, Vol. 173, (2016), 395-403, doi: 10.1016/j.matchemphys.2016.02.028
52. Henao, J., Poblano-Salas, C., Monsalve, M., Corona-Castuera, J., Barceinas-Sanchez, O.J.J.o.M.R. and Technology, "Bio-active glass coatings manufactured by thermal spray: A status report", ***Journal of Materials Research and Technology***, Vol. 8, No. 5, (2019), 4965-4984, doi: 10.1016/j.jmrt.2019.07.011
53. Odhiambo, J.G., Li, W., Zhao, Y. and Li, C.J.C., "Porosity and its significance in plasma-sprayed coatings", ***Coatings***, Vol. 9, No. 7, (2019), 460, doi: 10.3390/coatings9070460

Persian Abstract

چکیده

تلاش‌های زیادی برای بهبود ویژگی‌های سطحی مواد زیستی با پوشش‌های مختلف صورت گرفته است. در این پژوهش، یک نوع پوشش محافظ دولایه HA/Al_2O_3-SiO_2 (با ۱۰، ۲۰ و ۳۰ درصد وزنی SiO_2) به روش پلاسما اسپری بر روی سطح تیتانیوم اعمال شد. ویژگی‌های سطحی پوشش اعمال‌شده به تفصیل مورد ارزیابی قرار گرفت تا اثربخشی این کار برای کاربردهای زیست‌پزشکی بررسی شود. نتایج نشان داد که پوشش‌های یکنواخت و دولایه پلاسما اسپری شده را می‌توان با موفقیت از طریق بهینه‌سازی پارامترها تهیه کرد. همچنین مشخص شد که زبری پوشش های دولایه با افزایش تعداد لایه های پوشش افزایش می یابد. رفتار خوردگی نمونه های پوشش داده شده و بدون پوشش با استفاده از آزمون های الکتروشیمیایی مورد ارزیابی قرار گرفت. مقایسه مقاومت به خوردگی نمونه ۲۰ درصد SiO_2 با نمونه دارای پوشش تک لایه HA و نمونه تیتانیوم فاقد پوشش، بهبود قابل توجهی را نشان می‌دهد. پوشش پیشنهادی توانایی‌های امیدوارکننده‌ای را برای کاربردهای زیست‌پزشکی نشان داد.